



Numerical modelling and experimental determination of the dynamic behaviour of composite structures

Brandon Cohen¹; Paul Dylejko²; Stephen Moore³; Andrew Phillips⁴

¹ Royal Melbourne Institute of Technology, Australia

^{2,3,4} Defence Science and Technology Organisation, Australia

ABSTRACT

Composite materials are finding increasing application in mechanical systems because of their desirable physical characteristics compared with metals; for example, high strength- and stiffness-to-weight ratios, and the potential for constructing complex shapes without joints or extensive machining. In addition, the dynamic behaviour of composite structures can be manipulated by judicious selection of their constituent materials and structural features. This study investigates the dynamic behaviour of fibre-reinforced polymer hydrofoils using finite element analysis and experimental modal analysis. Four hydrofoils were made from different combinations of carbon, glass and aramid fibres to assess the influence of fibre type and fibre orientation on the hydrofoil's dynamic response. Numerical and experimental results showed good agreement for low-order modes. However, the results highlighted difficulties in determining higher-order modes accurately in both the numerical and experimental investigations. Fibre type and orientation were shown to appreciably affect the dynamic properties of the hydrofoil.

Keywords: Vibration, Composite Structures, Finite Element Analysis (FEA)
I-INCE Classification of Subjects Number(s): 42

1. INTRODUCTION

Composite materials are finding increasing use in maritime applications due to their many advantages compared with their metallic counterparts. These include increased strength- and stiffness-to weight ratios, corrosion resistance and the potential to produce complex shaped components without joints or excessive machining (1). Some of the most demanding applications in the maritime domain are cantilevered structures such as off-shore wind turbine blades or the rudders, keels, control surfaces and propellers of ships. It is vital that the dynamic response of these structures can be accurately predicted during the design phase so as to avoid potential issues with phenomena associated with resonance. To achieve this goal a detailed understanding of the factors that influence the natural frequencies, mode shapes and material damping properties of composite structures is required. Additionally, this modelling capability allows for component optimisation to further improve performance.

The dynamic properties of composites are influenced by fibre type and orientation. Kramer et al. (2) and Motley et al. (3) analysed the free vibration characteristics of cantilevered plates made from uniaxial layers of carbon fibre in both air and water. Their results showed that the mode shape can be appreciably influenced by changing the fibre orientation, particularly for modes greater than the first order. The change in mode shape was ascribed to an elastic coupling between bending and torsional modes (bend-twist coupling) induced by material anisotropy. Changing the fibre orientation has also been shown to influence the damping properties of the composites with higher damping occurring when fibres are not aligned along the principal loading direction (4-6). The use of certain fibre types such as aramid fibres (4, 7) as well as the use two or more combinations of reinforcement material (7)

¹ s3322221@student.rmit.edu.au

² paul.dylejko@dsto.defence.gov.au

³ stephen.moore@dsto.defence.gov.au

⁴ andrew.phillips@dsto.defence.gov.au

(hybridisation) have also been shown to increase the damping properties of composite structures. Accordingly, the dynamic properties of composite structures can be manipulated by judicious selection of their constituent materials and structural features.

The objective of this work was to investigate the free vibration characteristics of four composite hydrofoils. The hydrofoil shape was selected as it contains many of the structural features such as hydrodynamic profile as well as thickness and width tapers found in real applications. An experimental modal analysis (EMA) was performed using laser vibrometer measurements of the four hydrofoils. The results from these tests were then compared with numerical results generated using the finite element analysis (FEA) software Abaqus. Finally, the effects of fibre orientation and material type on the mode shape, natural frequency and structural damping characteristics of the hydrofoils were examined.

2. COMPOSITE HYDROFOIL MANUFACTURE

The chosen hydrofoil shape was an unswept trapezoid with the geometry shown in Figure 1 below. The hydrodynamic profile was a modified version of the NACA009 airfoil with a thicker trailing edge (1.59 mm at the root and 0.79 mm at the tip) to assist the manufacturing process.

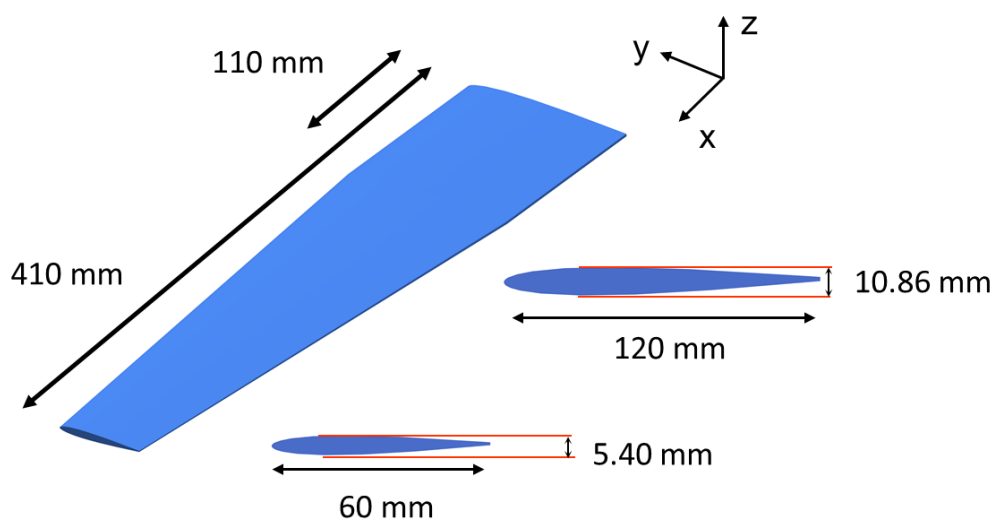


Figure 1 – Schematic diagram showing the main geometric features of the four composite hydrofoils used in this study.

Four hydrofoils were manufactured with different combinations of fabric materials and fibre orientations. All four foils had a fine 130 g/m² E-glass basket weave fabric as the outer-most layer to assist in achieving a high quality consistent surface finish. Additionally, all four foils had a 780 g/m² glass mat layer consisting of two 300 g/m² chopped strand mat skins and a 180 g/m² polyolefin scaffold core placed in their core to aid the infusion process. The difference between the four hydrofoils was in their structural layers, which impart the majority of the static strength and also significantly affect the dynamic behaviour of the structure.

Table 1 describes the layup of the structural layers at the root of the foils as well as their produced mass, density and root and tip thicknesses. The fabrics used to construct the structural layers were a 300 g/m² T-700 unidirectional carbon fibre, 600 g/m² E-glass biaxial fabric and 350 g/m² aramid basket weave fabric. The structural layers were symmetrically arranged about the mid-plane of the foils. The first two foils were a hybrid of uniaxial carbon and biaxial glass layers. The first foil had the unidirectional carbon fabric aligned along the longitudinal axis of the foil (GC00). The second foil had the uniaxial carbon layer offset by 30° toward the leading edge of the hydrofoil (GC30). The third foil was made from unidirectional carbon layers arranged in a quasi-isotropic layup (CCiso). The structural layers of the final foil were a hybrid of uniaxial carbon and basket weave aramid fabrics with the unidirectional carbon layers aligned with the longitudinal axis (AC00).

Table 1 – Summary of the layup of the structural layers of the four hydrofoils. Unidirectional carbon, biaxial glass and aramid fabrics represented by the subscripts *c*, *g* and *a*; numerical subscripts indicate the number of fibre layers; and S denotes the structural layers are symmetric around the foil mid-plane.

	GC00	GC30	CCiso	AC00
Layup of the structural layers at the foil root	$[(0^\circ/90^\circ)_g, 0^\circ_{5c}, (0^\circ/90^\circ)_{2g}, 0^\circ_{4c}]S$	$[(0^\circ/90^\circ)_g, 30^\circ_{5c}, (0^\circ/90^\circ)_{2g}, 30^\circ_{4c}]S$	$[(0^\circ/-45^\circ_c, 90^\circ/45^\circ_c)_3]S$	$[(0^\circ/90^\circ)_a, 0^\circ_{5c}, (0^\circ/90^\circ)_a, 0^\circ_{4c}]S$
Mass (g)	409.6	400.8	400.0	374.2
Density (g/cm³)	1.56	1.53	1.53	1.43
Max root thickness (mm)	10.79	10.76	10.77	10.70
Max tip thickness (mm)	5.44	5.40	5.63	5.43

To achieve the hydrodynamic profile and longitudinal thickness taper, the plies needed to be dropped. The structural plies were systematically dropped internally with the largest plies being on the outer surface and the smallest in the middle.

A closed mould resin transfer moulding (RTM) processes was used to manufacture the hydrofoils. The resin was a long pot-life two-part epoxy system (Kinetix R118/H103) specifically designed for infusion processes. Resin infusion took place under vacuum at room temperature with the infusion time generally less than 5 minutes. After infusion the foils were left to gel under a pressure of 1 bar. The parts were then post-cured at 100 °C for 4 hours. Finally, any flashing from the moulding process was manually ground off and the foils were weighed and their dimensions measured.

3. EXPERIMENTAL MODAL ANALYSIS

The four hydrofoils were tested in an approximately free-free condition supported by rubber bands as shown in Figure 2. The frequencies of the six rigid body modes were measured to be sufficiently below the frequency of the first elastic mode of the hydrofoils so as not to significantly influence the low-order elastic modes. The free-free condition was chosen because it could be achieved relatively easily; the cross-section of the hydrofoil made it difficult to clamp the root securely to achieve a fixed boundary condition.



Figure 2 – The hydrofoil supported by rubber bands is indicated and the loudspeaker is directly behind the hydrofoil. The three laser vibrometer heads are in the foreground.

A loudspeaker located 10 mm behind the hydrofoil and driven by a pseudo-random sequence was used as an excitation source. A Polytec PSV-400 3D laser vibrometer was used to measure the response of each hydrofoil at 127 points. A velocity spectrum between 0.625 – 2000 Hz with a resolution of 0.625 Hz was calculated for each measurement point by the vibrometer and a frequency response function (FRF) was also calculated using the pseudo-random sequence as a reference signal. Up to eight averages were calculated for each measurement point. It is emphasized that the FRFs were calculated using the pseudo-random sequence and not by an applied force or a microphone measurement of the acoustic excitation.

Modal parameters of the hydrofoils were estimated using two algorithms. The first was the PolyMAX experimental modal analysis tool in the LMS Test.Lab suite of software. This algorithm estimated the modal parameters from the FRFs. The second algorithm was the PolyMAX operational modal analysis tool in the LMS Test.Lab software, which used auto- and cross-spectra of the velocity response measurements. The results of the two approaches were compared and there was very good agreement between the estimated modal frequencies. Damping estimates were typically within 20%, noting that the magnitudes of the damping estimates, in terms of fraction of critical damping, were less than 0.01. The mode shapes estimated by the operational modal analysis algorithm (i.e. from cross spectra) were less clear than those estimated by the experimental modal analysis algorithm (i.e. from FRFs) and this was verified by examining the orthogonality of the estimated mode shapes using the modal assurance criterion (8). The mode shapes estimated from FRFs displayed a much greater degree of orthogonality compared with the mode shapes estimated by operational modal analysis, as shown for hydrofoil GC00 in Figure 3. In addition, FRFs synthesised using the experimental modal analysis results were similar to the measured FRFs as shown in Figure 4 for two measurement points on GC00. The results from the experimental modal analysis were used as a basis for comparison with the results from finite element analysis. It is acknowledged that some error in the experimental results was introduced because the reference for calculating the FRFs was not strictly the force applied to the structure.

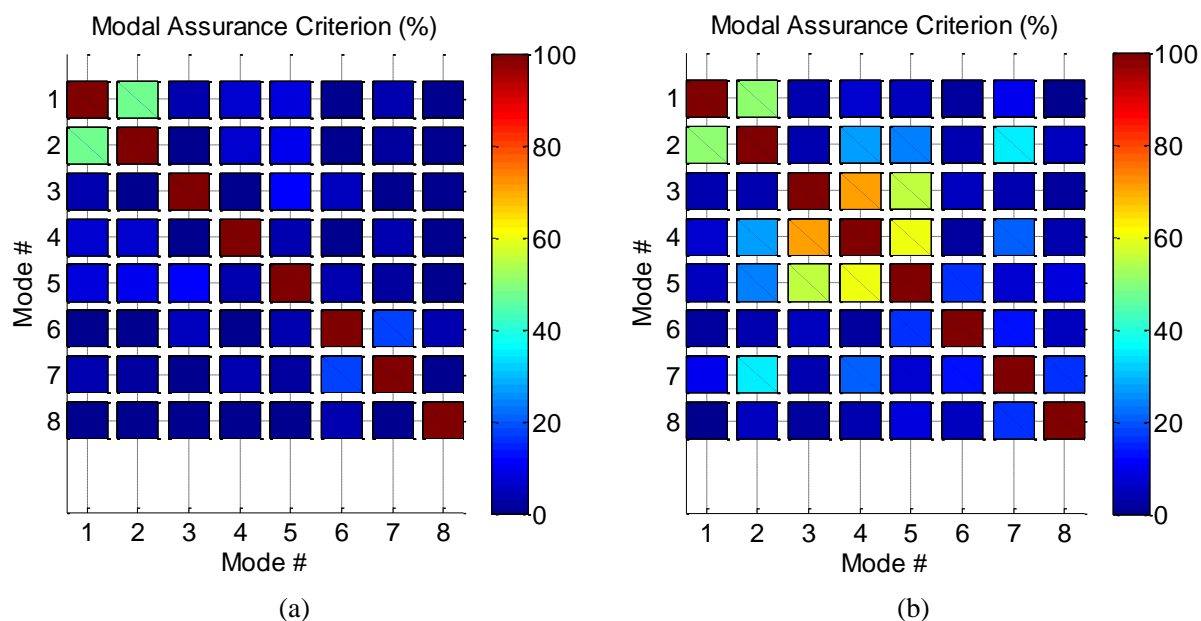


Figure 3 – Auto-modal assurance criterion for hydrofoil GC00; (a) experimental modal analysis results; (b) operational modal analysis results.

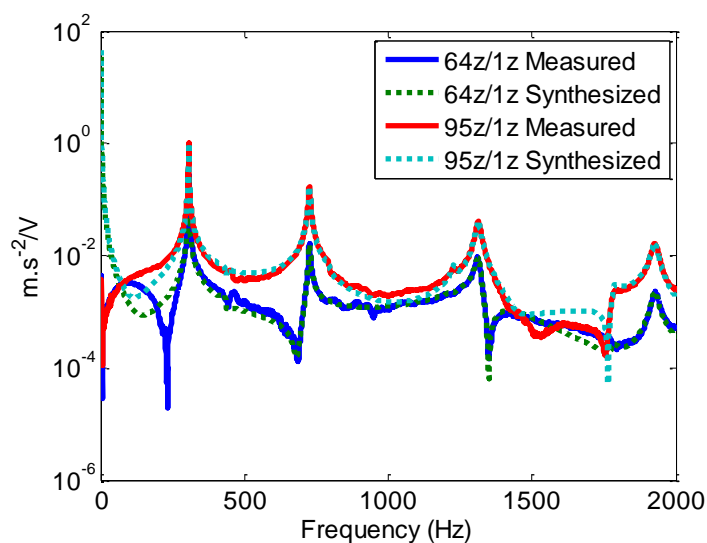


Figure 4 – Measured and synthesized FRFs for two points on GC00. Point 64 was close to the middle of the hydrofoil and point 95 was close to the corner between the tip and the trailing edge of the hydrofoil.

Table 2 – Natural frequencies and damping estimated from frequency response functions.

Mode	GC00		GC30		CCIso		AC00	
	Frequency (Hz)	Damping (%)						
1	306.2	0.18	184.2	0.55	334.5	0.16	304.7	0.29
2	433.5	1.02	473.4	0.51	468.7	0.68	416.5	0.98
3	726.0	0.37	708.3	0.61	740.9	0.68	755.1	0.52
4	793.5	0.87	1197	0.62	850.0	0.25	767.9	0.66
5	1230	0.77	1434	0.48	1285	0.54	1215	0.7
6	1313	0.6	1714	0.59	1555	0.29	1325	0.63
7	1782	0.67	-	-	1885	0.42	1809	0.62
8	1927	0.57	-	-	-	-	1928	0.69

Table 2 lists the modal frequencies and damping estimated from the FRFs for each hydrofoil, and the mode shapes for the first five modes for each hydrofoil are shown in Table A1 (Appendix A). The first mode estimated for each hydrofoil involved bending with half a wavelength along the hydrofoil span. Comparison of the first modal frequencies for the GC00 and GC30 hydrofoils shows that orientating the carbon fibres at 30° to the hydrofoil's longitudinal axis reduced the natural frequency from 306.2 Hz to 184.2 Hz. This is a significant change of natural frequency noting that the mass of GC30 was within 10 grams of the mass of the GC00. The modal frequency of mode 2 is similar for each hydrofoil as was the modal frequency for mode 3.

Mode 2 of GC00 (433.5 Hz) had torsional deformation with one node and this shape also occurred in the second mode of AC00 (416.5 Hz), the third mode of both CCIso (740.9 Hz), and the third mode of GC30 (708.3 Hz). The second mode of GC30 (473.4 Hz) had bending with one wavelength along the span and this deformation corresponded to the third mode shape of GC00 (726.0 Hz). Hence the shapes of modes 2 and 3 in GC00 and GC30 have been transposed while the corresponding frequencies of modes 2 and 3 are within 10%. AC00 had the same carbon fibre orientation as GC00 and this accounts for the reasonable degree of similarity of mode shapes for these two hydrofoils. The deformation of higher order modes in each hydrofoil was a combination of bending and torsion affected by the non-symmetrical cross-section, variation of the chord length along the hydrofoil span, and the structural plies.

The damping of the modes estimated for each hydrofoil was typically less than 1%. The average damping across all modes was similar for the GC00 and AC00 hydrofoils (~0.63%); GC30 had slightly

lower average damping (~0.56 %) and CCIso had the lowest average damping (~0.43 %). It was observed that modes with bending deformation had marginally lower damping than modes with torsional deformation. It is acknowledged that damping estimates can have a significant variance and more careful measurement of the structural damping would be necessary to verify any trend in damping.

Acoustic excitation of a free-free hydrofoil was a relatively simple method of excitation compared with shaker excitation of a hydrofoil with a fixed boundary condition. In addition, the acoustic excitation allowed the laser vibrometer to be set to measure a large number of points quickly compared with impact hammer excitation. However, the loudspeaker was only able to provide a low-level excitation force compared with impact hammer excitation or shaker excitation and the distributed acoustic excitation may not have effectively excited higher order modes. It is envisaged that further studies on the dynamic behaviour of composite hydrofoils will investigate the response to larger excitation levels and also determine the influence of amplitude-dependent non-linearity in the hydrofoils. A fixed boundary condition on the hydrofoil and use of a grounded shaker would allow more precise alignment and control of the excitation force.

4. FINITE ELEMENT MODELLING

The natural frequencies of the four hydrofoils were numerically determined using the commercial FEA software Abaqus. A number of parametric studies were performed to determine appropriate element types and mesh density. SC8R elements were selected from the results of the parametric studies due to their balance of high computational efficiency and reasonable accuracy in prediction of dynamic behaviour. The foils were modelled using 52704 linear hexahedron (SC8R-reduced integration continuum shells) elements. A free-free boundary condition was applied to allow direct comparison with the experimental results. Lamina material models were used to describe the elastic properties of the different fabrics, and these are summarised in Table 3. The material properties were based on coupon test results of the material or if these were unavailable results derived from similar materials produced under similar conditions. The Abaqus add-on package Composite Modeler was used to numerically reproduce the layup sequence of each hydrofoil including the locations of the ply drops. A summary of the mode shapes and natural frequencies determined from FEA is provided in Table A2 in Appendix A.

Table 3 – Summary of the material properties used in the finite element analysis

Material	Density (g/cm ³)	E ₁₁ (MPa)	E ₂₂ (MPa)	ν_{12}	G ₁₂ (MPa)
300Carbon-UD	1.55	118000	6500	0.27	4500
Glass-(0/90)	1.78	20600	20600	0.32	4000
Glass-Basket	1.69	15000	15000	0.13	4000
Glass-Mat	1.38	5000	5000	0.26	4000
Kevlar-Basket	1.30	30000	30000	0.2	5000
Resin	1.2	3271		0.3	

5. COMPARISON OF EXPERIMENTAL AND FINITE ELEMENT MODEL RESULTS

Table 4 compares the modal frequencies estimated from experimental modal analysis and finite element analysis. The modes were paired on the basis of frequency and mode shape, and mode pairs with a reasonable degree of correlation in the mode shapes are highlighted in the table. There is good agreement between the first four modes of GC00 and the first three modes of GC30, which demonstrates that fibre orientation can be modelled to a satisfactory degree. In all cases the level of correlation between EMA and FEA results decreased above 800 Hz. The results for the CCIso and AC00 hydrofoils showed reasonable agreement between measured and predicted mode shapes; however, there were differences of greater than 10% between the measured and predicted natural frequencies.

The cause of the observed discrepancies between FEA and EMA results may lie in the assumptions used to create the FE models. The most significant among these is the accuracy of the material models and the numerical representation of the layup sequence used. Follow-up studies are currently being performed to determine the in-plane elastic properties of the constituent materials as well as the achieved ply thicknesses and fibre volume fractions. Another source of uncertainty is the use of thick shell composite elements. Although being computationally efficient these elements are unable to adequately account for through-thickness stress states which develop when the foils undergo bending or torsion leading to a somewhat stiffer response than would otherwise be expected.

Table 4 – Comparison of modal frequencies estimated from experimental modal analysis (EMA) and finite element analysis (FEA). The shaded cells indicate modes with correlated mode shapes.

GC00			GC30		
Frequency (Hz)		% error	Frequency (Hz)		% error
EMA	FEA	re EMA	EMA	FEA	re EMA
306.2	289.9	-5.3	184.2	177.2	-3.8
433.5	425.5	-1.8	473.4	445.6	-5.9
726.0	716.1	-1.4	708.3	665.0	-6.1
793.5	760.1	-4.2	1197	827.8	-30.8
1230	1176		1434	1120	

CCIso			AC00		
Frequency (Hz)		% error	Frequency (Hz)		% error
EMA	FEA	re EMA	EMA	FEA	re EMA
334.5	284.2	-15.0	304.7	332.1	9.0
468.7			416.5	509.1	22.2
740.9	748.3	1.0		833.2	
850.0	714.4	-15.9	755.1	912.6	20.9
1285	1257	-2.2	767.9	1415.5	84.3
	1343		1215		

6. CONCLUSIONS

The dynamic behaviour of fibre-reinforced polymer hydrofoils has been investigated using finite element analysis and experimental modal analysis. Four hydrofoils were examined which were made from different combinations of carbon, glass and aramid fibres to assess the influence of fibre type and fibre orientation on the hydrofoil's dynamic response. Numerical and experimental results showed good agreement for low-order modes, which suggests that finite element modelling could be used to optimise the low frequency behaviour in composite structures. Results highlighted difficulties in determining higher-order modes accurately in both the numerical and experimental investigations. The acoustic excitation used in the experimental study may not have adequately excited the higher-order modes and the material properties and modelling of the fibre layup are two potential sources of error in the finite element analysis. Fibre type and orientation were shown to appreciably affect the dynamic properties of the hydrofoil and further studies are planned to investigate how the composite properties affect structural damping.

ACKNOWLEDGEMENTS

The authors wish to thank Dr Nigel St. John, Mr Russell Cairns and Dr Asintha Nanayakkara from the Defence Science and Technology Organisation (DSTO) for their assistance in the manufacture of the hydrofoils.

REFERENCES

1. Mouritz, AP, Gellert E, Burchill P, Challis K, Review of advanced composite structures for naval ships and submarines. *Composite Structures*. 2001;53:21-42
2. Kramer MR, Liu Z, Young YL. Free vibration of cantilevered composite plates in air and in water. *Composite Structures*. 2012;95:254-263
3. Motley MR, Kramer MR, Young YL. Free surface and solid boundary effects on the free vibration of cantilevered composite plates. *Composite Structures*. 2013;96:365–375.
4. Berthelot J-M, Sefrani Y. Damping analysis of unidirectional glass and Kevlar fibre composites. *Composite Science and Technology*. 2004;64:1261–1278
5. Mahi AE, Assarar M, Sefrani Y, Berthelot J-M, Damping analysis of orthotropic composite materials and laminates. *Composites Part B: Engineering*. 2008;39:1069–1076
6. Chaturvedi SK. Damping Characterization of Polymer Matrix Composite Materials. In *Wiley Encyclopedia of Composites*. John Wiley and Sons; 2012. p 1-15.
7. Chaviaropoulos P.K, Politis ES, Lekou DJ, Sørensen NN, Hansen MH, Bulder BH, Windelaar D, Lindenburg C, Saravanos DA, Philippidis TP, Galiotis C, Hansen MOL, Kossivas T. Enhancing the damping of wind turbine rotor blades, the DAMPBLADE project. *Wind Energy*. 2006;9:163-177.
8. Maia NMM, Silva JMM, editors. *Theoretical and experimental modal analysis*: Research Studies Press Ltd.; 1997.

Appendix A Mode Shapes from Experiments and Finite Element Analysis

Table A1 – Mode shapes, natural frequencies, and damping estimated from experimental measurements.

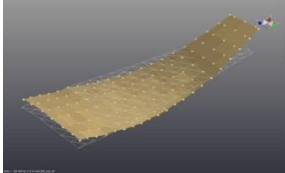
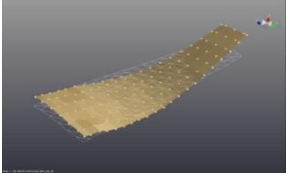
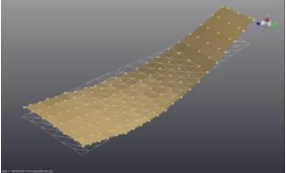
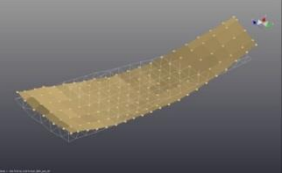
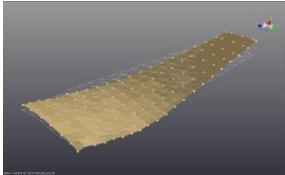
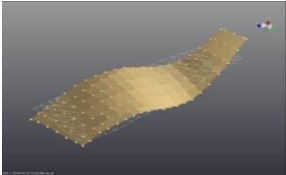
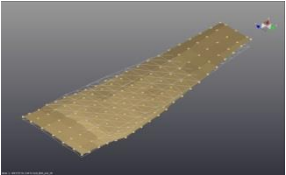
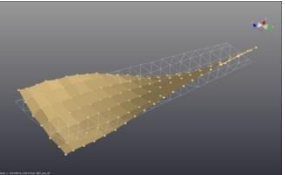
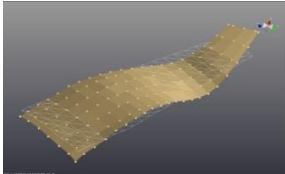
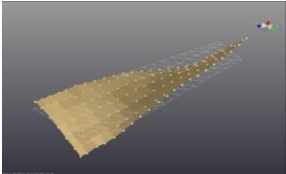
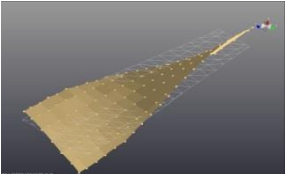
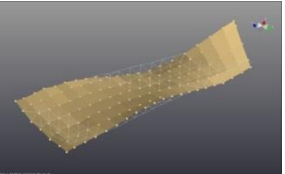
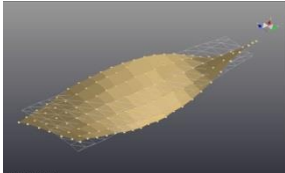
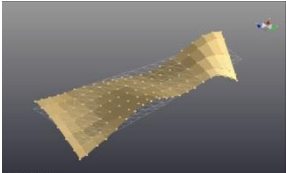
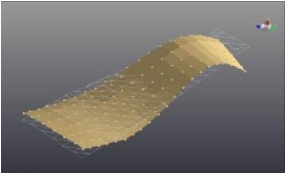
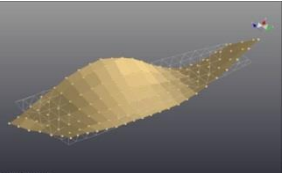
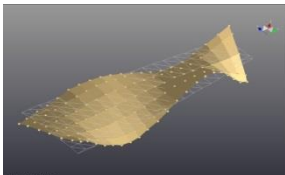
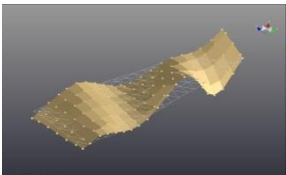
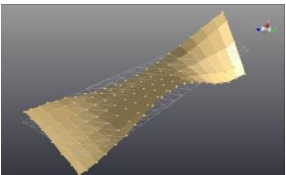
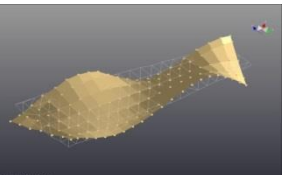
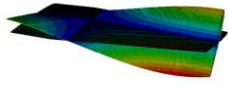
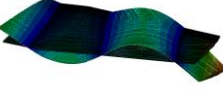
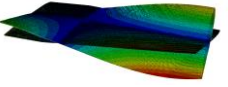
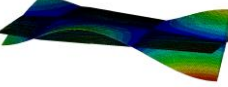
GC00		GC30		CCIso		AC00	
306.2 Hz	0.18 %	184.2 Hz	0.55 %	334.5 Hz	0.16 %	304.7 Hz	0.29 %
							
433.5 Hz	1.02 %	473.4 Hz	0.51 %	468.7 Hz	0.68 %	416.5 Hz	0.98 %
							
726.0 Hz	0.37 %	708.3 Hz	0.61 %	740.9 Hz	0.68 %	755.1 Hz	0.52 %
							
793.5 Hz	0.87 %	1197 Hz	0.62 %	850.0 Hz	0.25 %	767.9 Hz	0.66 %
							
1230 Hz	0.77 %	1434 Hz	0.48 %	1285 Hz	0.54 %	1215 Hz	0.7 %
							

Table A2 – Mode shapes and natural frequencies estimated from finite element analysis.

GC00	GC30	CCIso	AC00
289.9 Hz	177.2 Hz	284.2 Hz	332.1 Hz
			
425.5 Hz	445.6 Hz	714.4 Hz	509.1 Hz
			
716.1 Hz	665.0 Hz	748.3 Hz	833.2 Hz
			
760.1 Hz	827.8 Hz	1257 Hz	912.6 Hz
			
1176 Hz	1120 Hz	1343 Hz	1416 Hz
